CHALMERS
FINITE ELEMENT CENTER

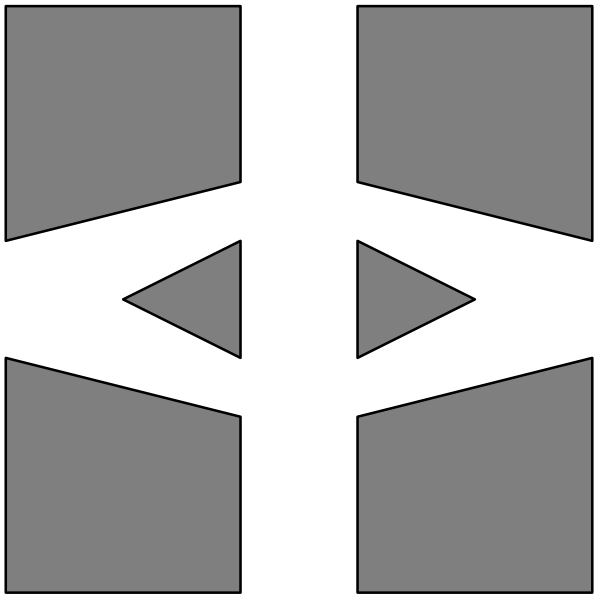

PREPRINT 2003–04

Crouzeix–Raviart and Raviart–Thomas elements for acoustic fluid–structure interaction

Joakim Hermansson

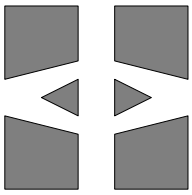

Chalmers Finite Element Center
CHALMERS UNIVERSITY OF TECHNOLOGY
Göteborg Sweden 2003

CHALMERS FINITE ELEMENT CENTER

Preprint 2003–04

Crouzeix–Raviart and Raviart–Thomas elements for acoustic fluid–structure interaction

Joakim Hermansson

CHALMERS

Chalmers Finite Element Center
Chalmers University of Technology
SE–412 96 Göteborg Sweden
Göteborg, February 2003

Crouzeix–Raviart and Raviart–Thomas elements for acoustic fluid–structure interaction
Joakim Hermansson
NO 2003–04
ISSN 1404–4382

Chalmers Finite Element Center
Chalmers University of Technology
SE–412 96 Göteborg
Sweden
Telephone: +46 (0)31 772 1000
Fax: +46 (0)31 772 3595
www.phi.chalmers.se

Printed in Sweden
Chalmers University of Technology
Göteborg, Sweden 2003

CROUZEIX–RAVIART AND RAVIART–THOMAS ELEMENTS FOR ACOUSTIC FLUID–STRUCTURE INTERACTION

JOAKIM HERMANSSON

ABSTRACT. We consider the eigenvalue problem arising from small vibration fluid–structure interaction. We propose using the lowest order Raviart–Thomas (RT) element for the linear fluid and the first order non-conforming Crouzeix–Raviart (CR) element for the linear elastic structure. The RT element, whose unknowns are the normal projection of the field variable on the element sides, are known to give solutions free from spurious nonzero frequency circulation modes The unknowns on the CR element are chosen as the normal and tangential projection of the field variable at each side node. This choice leads to that the normal degrees of freedom on the interface will be the same for the structure and the fluid as long as the meshes match on the interface. Further, a consistent stabilizing term is added to the weak form to make the CR element stable for elasticity. An additional benefit of the CR element is that is does not lock for near incompressible materials.

1. INTRODUCTION

Small vibration fluid–structure interaction (FSI) in enclosed cavities, appears, for instance, in vehicle compartments (cars, aircrafts, trains) or in buildings. Of special interest are the eigenfrequencies and the corresponding eigenmodes of the coupled fluid–structure system, since excitation of these modes may result in unwanted noise. To avoid such phenomena, it is important already in the design process to predict the eigenfrequencies of the coupled system with some numerical tool. Further, it can be of interest to predict the sound pressure level, due to some given excitation, which can preferably be done with a modal analysis approach. Here we will deal with a finite element (FE) formulation to solve the eigenvalue problem, using the lowest order Raviart–Thomas (RT) elements for the linear fluid, and the first order non-conforming Crouzeix–Raviart (CR) elements for the linear elastic structure.

An attractive approach to discretize the fluid is to use standard (continuous) finite elements. Unfortunately, this leads to spurious nonzero frequency modes, see, e.g., Hamdi et al. [1]. A displacement formulation that avoids spurious nonzero frequency modes was introduced in Bermúdez et al. [2, 3], where the fluid displacements were discretized with the

Date: February 11, 2003.

Key words and phrases. Fluid–structure interaction,Crouzeix–Raviart elements, Raviart–Thomas elements.

Joakim Hermansson, Department of Applied Mechanics, Chalmers University of Technology, SE–412 96 Göteborg, Sweden, *email*:joakim.hermansson@me.chalmers.se

This work was supported by the Swedish Foundation for Strategic Research through the Integral Vehicle Structure (IVS) graduate school.

lowest order Raviart–Thomas element, on which the unknowns are the normal projection of the field variable on the element sides, see, e.g., Ewing and Sævareid [4]. If standard finite elements are used to describe the structural displacements, conditions which relate the unknowns of the fluid and the structure on the interface have to be introduced, since the positions of the unknowns will not match on the interface. To quote Wang and Bathe [9], referring to the Raviart–Thomas elements: "This formulation is promising but the degrees of freedom of the fluid elements are not those of the structure and the coupling needs special considerations".

Here we suggest to discretize the structure using the first order Crouzeix–Raviart element and defining the unknowns as the normal and tangential projection of the displacement at each side node. Thus, using the Raviart–Thomas element for the fluid, the normal displacement degrees of freedom on the interaction boundaries are the same for the fluid and the structure, as long the meshes match on the interfaces. Since the unknowns on the CR elements are located at the center of gravity on the element sides, the elements can rotate around the side nodes violating Korn's inequality for elasticity. In order to stabilize the element, a consistent stability term is added to the weak form, as suggested in Hansbo and Larson [5, 6] (see Brenner [7] for a proof of Korn's inequality using this stabilization method). The optimal magnitude of the stabilizing term is investigated by a numerical example. Further, a numerical example is given with the proposed fluid–structure interaction method. We remark that an additional benefit of the proposed version of the CR element is that it does not lock for near incompressible materials. We also give a numerical example showing this property.

2. The fluid–structure interaction problem

The problem we aim to solve is the eigenvalue problem originating from the interaction between a linear fluid enclosed in a linear elastic structure. The fluid domain is denoted Ω_{F}, the structural domain Ω_{S} and the interaction boundary Γ. The exterior structural boundary is divided in two parts, Γ_{D} and Γ_{N}. The displacements are prescribed on Γ_{D} while the traction is prescribed on Γ_{N}. The governing equations for the continuous fluid–structure problem expressed in the frequency domain reads:

$$\nabla p - \omega^2 \rho_{\mathrm{F}} \boldsymbol{u}_{\mathrm{F}} = \boldsymbol{0} \qquad \text{in } \Omega_{\mathrm{F}}, \tag{2.1}$$

$$p + c^2 \rho_{\mathrm{F}} \nabla \cdot \boldsymbol{u}_{\mathrm{F}} = 0 \qquad \text{in } \Omega_{\mathrm{F}}, \tag{2.2}$$

$$\nabla \cdot \boldsymbol{\sigma} + \omega^2 \rho_{\mathrm{S}} \boldsymbol{u}_{\mathrm{S}} = \boldsymbol{0} \qquad \text{in } \Omega_{\mathrm{S}}, \tag{2.3}$$

$$\sigma_n + p = 0 \qquad \text{on } \Gamma, \tag{2.4}$$

$$(\boldsymbol{u}_{\mathrm{F}} - \boldsymbol{u}_{\mathrm{S}}) \cdot \boldsymbol{n} = 0 \qquad \text{on } \Gamma, \tag{2.5}$$

$$\boldsymbol{\sigma}_t = \boldsymbol{0} \qquad \text{on } \Gamma, \tag{2.6}$$

$$\boldsymbol{n}_{\mathrm{S}} \cdot \boldsymbol{\sigma} = \boldsymbol{0} \qquad \text{on } \Gamma_{\mathrm{N}}, \tag{2.7}$$

$$\boldsymbol{u}_{\mathrm{S}} = \boldsymbol{g} \qquad \text{on } \Gamma_{\mathrm{D}}, \tag{2.8}$$

where $\boldsymbol{u}_{\mathrm{F}}$ and $\boldsymbol{u}_{\mathrm{S}}$ are the fluid and structural displacements, respectively, and p is the fluid pressure. Further, ω is the angular frequency, c is the speed of sound, and ρ_{F} and ρ_{S} are the fluid and the structural density, respectively. The stress tensor, $\boldsymbol{\sigma}$, is given by Hooke's law as $\sigma_{ij} = \lambda\delta_{ij}\nabla\cdot\boldsymbol{u}_{\mathrm{S}} + 2\mu\varepsilon_{ij}(\boldsymbol{u}_{\mathrm{S}})$, where δ_{ij} is the Kronecker delta, λ and μ are the Lamé constants, and

$$\varepsilon_{ij}(\boldsymbol{u}) = \frac{1}{2}\Big(\frac{\partial u_i}{\partial x_j} + \frac{\partial u_j}{\partial x_i}\Big). \tag{2.9}$$

The Lamé constants are given as $\mu = E/[2(1+\nu)]$ and $\lambda = E\nu/[(1+\nu)(1-2\nu)]$, where E is Young's modulus and ν is Poisson's ratio. Finally, $\sigma_n = \boldsymbol{n}_{\mathrm{S}}\cdot(\boldsymbol{n}_{\mathrm{S}}\cdot\boldsymbol{\sigma})$ is the normal stress on Γ, $\boldsymbol{\sigma}_t = \boldsymbol{n}_{\mathrm{S}}\cdot\boldsymbol{\sigma} - \sigma_n\boldsymbol{n}_{\mathrm{S}}$ is the tangential traction vector on Γ, $\boldsymbol{n}$ is the outward pointing normal to Ω_{F}, and $\boldsymbol{n}_{\mathrm{S}}$ is the outward pointing normal to Ω_{S}.

3. The finite element formulation

The triangulation of Ω_{S} is denoted $\mathcal{T}_{\mathrm{S}}$ and the triangulation of Ω_{F} is denoted $\mathcal{T}_{\mathrm{F}}$. Further, $\mathcal{E}_{\mathrm{I}}$ contains the interior element sides E on Ω_{S}, and $\mathcal{E}_{\mathrm{D}}$ contains the element sides E located on the prescribed displacement boundary Γ_{D}. To each element side E there is an associated predefined side normal vector $\boldsymbol{n}_E$. Next, we define the Crouzeix–Raviart finite element space as

$$\begin{aligned} CR(\Omega_{\mathrm{S}}) = \{\boldsymbol{v}\in L_2(\Omega_{\mathrm{S}}) : \boldsymbol{v}|_K \in [P_1(K)]^2 \quad &\forall \text{ element } K\in\mathcal{T}_{\mathrm{S}},\\ &\boldsymbol{v} \text{ is continuous at the center of gravity of the element sides}\},\end{aligned}$$

where $L_2(\Omega) = \{\boldsymbol{v} : \int_\Omega \boldsymbol{v}\cdot\boldsymbol{v}\,\mathrm{d}\Omega < \infty\}$ and $[P_1(K)]^2$ denotes a 2-dimensional vector containing linear polynomials defined on K. The Raviart–Thomas finite element space is defined as

$$\begin{aligned} RT(\Omega_{\mathrm{F}}) = \{\boldsymbol{v}\in H(\mathrm{div},\Omega_{\mathrm{F}}) : \boldsymbol{v}|_K = (a+bx, c+by),\ a,b,c\in\mathbb{R}\\ \forall \text{ element } K\in\mathcal{T}_{\mathrm{F}}, \boldsymbol{v}\cdot\boldsymbol{n} \text{ is cont. and const. on the element sides}\},\end{aligned}$$

where $H(\mathrm{div},\Omega_{\mathrm{F}}) = \{\boldsymbol{v}\in L_2(\Omega) : \nabla\cdot\boldsymbol{v}\in L_2(\Omega)\}$. The finite dimensional function space to the given problem, with the interface condition invoked, follows as

$$\begin{aligned}\mathcal{V}_h = \{(\boldsymbol{v}_{\mathrm{F}},\boldsymbol{v}_{\mathrm{S}})\in RT\times CR : \int_E (\boldsymbol{v}_{\mathrm{F}}-\boldsymbol{v}_{\mathrm{S}})\cdot\boldsymbol{n}\,\mathrm{d}E = 0\\ \forall E\in\Gamma\}.\end{aligned}$$

For our choice of element approximations, this means that the normal displacement degrees of freedom, on the interface, are the same for the fluid and the structure. We emphasize that this is an important property from an implementation point of view (higher order versions of the RT and CR elements have the same property).

Our nonconforming finite element formulation for the fluid–structure interaction problem can now be written: find $\boldsymbol{U} = (\boldsymbol{U}_{\mathrm{F}},\boldsymbol{U}_{\mathrm{S}})\in\mathcal{V}_h$ and $\omega_h\in\mathbb{R}_+$ such that

$$a_h(\boldsymbol{U},\boldsymbol{v}) = \omega_h^2 b_h(\boldsymbol{U},\boldsymbol{v}) \qquad \forall\boldsymbol{v} = (\boldsymbol{v}_{\mathrm{F}},\boldsymbol{v}_{\mathrm{S}})\in\mathcal{V}_h, \tag{3.1}$$

where

$$
\begin{aligned}
a_h(\boldsymbol{U},\boldsymbol{v}) &= \sum_{K\in\mathcal{T}_\mathrm{S}} \int_K \left[\lambda\nabla\cdot\boldsymbol{U}_\mathrm{S}\nabla\cdot\boldsymbol{v}_\mathrm{S} + 2\mu\boldsymbol{\varepsilon}(\boldsymbol{U}_\mathrm{S}):\boldsymbol{\varepsilon}(\boldsymbol{v}_\mathrm{S})\right]\mathrm{d}\Omega \\
&\quad + C\sum_{E\in\mathcal{E}_\mathrm{I}\cup\mathcal{E}_\mathrm{D}} \int_E \frac{1}{h_E}\Big(2\mu[\![\boldsymbol{U}_\mathrm{S}]\!]\cdot[\![\boldsymbol{v}_\mathrm{S}]\!] + \lambda[\![\boldsymbol{U}_\mathrm{S}\cdot\boldsymbol{n}_E]\!]\,[\![\boldsymbol{v}_\mathrm{S}\cdot\boldsymbol{n}_E]\!]\Big)\mathrm{d}E \\
&\quad + \rho_\mathrm{F}c^2\int_{\Omega_\mathrm{F}} \nabla\cdot\boldsymbol{U}_\mathrm{F}\nabla\cdot\boldsymbol{v}_\mathrm{F}\,\mathrm{d}\Omega, \\
b_h(\boldsymbol{U},\boldsymbol{v}) &= \rho_\mathrm{F}\int_{\Omega_\mathrm{F}} \boldsymbol{U}_\mathrm{F}\cdot\boldsymbol{v}_\mathrm{F}\,\mathrm{d}\Omega + \rho_\mathrm{S}\int_{\Omega_\mathrm{S}} \boldsymbol{U}_\mathrm{S}\cdot\boldsymbol{v}_\mathrm{S}\,\mathrm{d}\Omega.
\end{aligned}
$$

The bracket $[\![\cdot]\!]$ denotes the jump on the element sides, and is defined as $[\![\boldsymbol{u}]\!] = \boldsymbol{u}^+ - \boldsymbol{u}^-$ for all $E \in \mathcal{E}_\mathrm{I}$. It does not matter on which side of the element sides $\boldsymbol{u}^+$ and $\boldsymbol{u}^-$ are defined since the jump term is symmetric. Further, $[\![\boldsymbol{U}_\mathrm{S}]\!] = \boldsymbol{U}_\mathrm{S}^+ - \boldsymbol{g}$ and $[\![\boldsymbol{v}_\mathrm{S}]\!] = \boldsymbol{v}_\mathrm{S}^+$ for all $E \in \mathcal{E}_\mathrm{D}$. The ω_h is the approximate ω and h_E is (here) the length of side E, but it can be chosen differently, see [5]. The optimal magnitude of the stability parameter C is investigated numerically in Section 5.1. The second part of the stability term has to be dropped if problems with near incompressible materials are going to be solved, since $\lambda \to \infty$ as $\nu \to 0.5$, and locking can occur. See a numerical example in Section 5.1. The first part of the first term, i.e., the λ-term, does not cause any problem when ν is close to 0.5 since the CR element can interpolate both the divergence and the displacement field, see Thomasset [8]. Note that when $\nu = 0.5$, i.e., incompressibility, $\nabla\cdot\boldsymbol{u}_\mathrm{S} = 0$.

4. Practical implementation

Structural domain: The elastic structure (2D) is discretized with first order non-conforming Crouzeix–Raviart elements, on which the unknowns are located at the center of gravity on the element sides, see Figure 1a. Here we have chosen to describe each nodal displacement by its normal and tangential component. The direction of a element side normal vector $\boldsymbol{n}_E$ (and thus the tangential vector) at a side node depends on its global definitions, i.e, the depicted directions at a side node in Figure 1a may be rotated 180°. The approximate displacements on a structural element follows as

$$\boldsymbol{U}_\mathrm{S} = \boldsymbol{\varphi}_\mathrm{S}\mathbf{U}_\mathrm{S},$$

where

$$\boldsymbol{\varphi}_\mathrm{S} = [\varphi_1\boldsymbol{n}_1 \quad \varphi_1\boldsymbol{t}_1 \quad \varphi_2\boldsymbol{n}_2 \quad \varphi_2\boldsymbol{t}_2 \quad \varphi_3\boldsymbol{n}_3 \quad \varphi_3\boldsymbol{t}_3]$$

contains the basis functions and the normal and tangential vector at each side node. The basis functions are those used for a standard linear triangle, but defined on the inscribed triangle, see Figure 1a. For instance, $\varphi_1 = 1$ at side node 1, and $\varphi_1 = 0$ at side node 2 and 3. Further, $\mathbf{U}_\mathrm{S} = [\mathrm{U}_n^1\ \mathrm{U}_t^1\ \mathrm{U}_n^2\ \mathrm{U}_t^2\ \mathrm{U}_n^3\ \mathrm{U}_t^3]^\mathrm{T}$ contains the normal and tangential displacement components at the side nodes. The structural element stiffness matrix is built up from the

first and the second term in the expression for $a_h(\boldsymbol{U}, \boldsymbol{v})$ in (3.1). The contribution from the first term to the structural element stiffness matrix is given by

$$\int_K \tilde{\nabla}\boldsymbol{\varphi}_{\mathrm{S}}^{\mathrm{T}} \boldsymbol{D} \tilde{\nabla}\boldsymbol{\varphi}_{\mathrm{S}} \mathrm{d}K,$$

where

$$\tilde{\nabla}\boldsymbol{\varphi}_{\mathrm{S}} = \begin{bmatrix} \dfrac{\partial\varphi_1}{\partial x_1} n_1^1 & \dfrac{\partial\varphi_1}{\partial x_1} t_1^1 & \cdots \\ \dfrac{\partial\varphi_1}{\partial x_2} n_2^1 & \dfrac{\partial\varphi_1}{\partial x_2} t_2^1 & \cdots \\ \left(\dfrac{\partial\varphi_1}{\partial x_2} n_1^1 + \dfrac{\partial\varphi_1}{\partial x_1} n_2^1\right) & \left(\dfrac{\partial\varphi_1}{\partial x_2} t_1^1 + \dfrac{\partial\varphi_1}{\partial x_1} t_2^1\right) & \cdots \end{bmatrix},$$

$\boldsymbol{D}$ is the constitutive matrix for plane strain, see Hughes [10], $\boldsymbol{n}_i = [n_1^i \; n_2^i]^{\mathrm{T}}$, $\boldsymbol{t}_i = [t_1^i \; t_2^i]^{\mathrm{T}}$ and $i = 1, 2, 3$ is the side node number. The second term (stabilizing), which contributes to the structural element stiffness matrix, give rise to that the bandwidth of the matrix will increase, compared to standard finite elements. In the interior of the mesh the belonging rows and columns in the stiffness matrix will contain 26 components (in 2D elasticity). For instance, the side node on E_1 in Figure 2 is coupled to all unknowns on the patch. This because the jump terms on the sides $E_2 - E_5$ will couple the unknowns at E_1 to the unknowns at the outer side nodes on the patch. This can be compared with about 12 components for standard linear elements if each interior node is surrounded by five elements. On the other hand, the consistent structural mass matrix (the second term of $b_h(\boldsymbol{U}, \boldsymbol{v})$ in (3.1)) will be diagonal. This can be verified by the fact that for the three point quadrature formula, which has its quadrature points on each midside node and integrates quadratic polynomials exactly on a triangle, we have that at each quadrature point one basis function is equal to one and the other two are equal to zero.

Fluid domain: The fluid domain (2D) is discretized using the lowest order Raviart–Thomas element, see Figure 1b, on which the unknowns are the normal projection of the field variable on each element side. The normal projections are constant along the element sides. The basis functions (vectors) on an element are given by, if the global element side normal $\boldsymbol{n}_E$ is pointing outward on E_i,

$$\boldsymbol{\varphi}_i = \frac{|E_i|}{2A}(\boldsymbol{x} - \boldsymbol{x}_{i'}),$$

and if the global element side normal $\boldsymbol{n}_E$ is positive inwards

$$\boldsymbol{\varphi}_i = -\frac{|E_i|}{2A}(\boldsymbol{x} - \boldsymbol{x}_{i'}),$$

where $i = 1, 2, 3$ is the side number, $|E_i|$ is the length of the element side i, A is the element area, and the $(')$ sign denotes the geometrical nodes. Further,

$$\boldsymbol{\varphi}_i \cdot \boldsymbol{n}_j = \delta_{ij} \quad \text{on } E_j,$$

where $i, j = 1, 2, 3$. Finally, the displacements on an element are approximated as

$$\boldsymbol{U}_{\mathrm{F}} = \boldsymbol{\varphi}_{\mathrm{F}} \mathbf{U}_{\mathrm{F}} = [\boldsymbol{\varphi}_1 \quad \boldsymbol{\varphi}_2 \quad \boldsymbol{\varphi}_3] \begin{bmatrix} \mathrm{U}_n^1 \\ \mathrm{U}_n^2 \\ \mathrm{U}_n^3 \end{bmatrix}.$$

5. Numerical studies

The following data will be used in all numerical examples:

$$\begin{aligned} \rho_{\mathrm{F}} &= 1000\,\mathrm{kg/m^3}, \\ c &= 1430\,\mathrm{m/s}, \\ \rho_{\mathrm{S}} &= 7700\,\mathrm{kg/m^3}, \\ E &= 144\,\mathrm{GPa}. \end{aligned}$$

5.1. **The stability parameter C.** The magnitude of the stability parameter C in the FE formulation, see (3.1), is investigated comparing the FE solution with the analytical solution to the model problem seen in Figure 3. The boundary and the volume forces are given by

$$\begin{aligned} \sigma_{22}(x_1, \frac{H}{2}) &= -2A\frac{H}{2}\frac{\nu E}{(1+\nu)(1-2\nu)}\ \mathrm{Pa}, \\ \sigma_{22}(x_1, -\frac{H}{2}) &= 2A\frac{H}{2}\frac{\nu E}{(1+\nu)(1-2\nu)}\ \mathrm{Pa}, \\ \sigma_{11}(B, x_2) &= -2Ax_2\frac{E(1-\nu)}{(1+\nu)(1-2\nu)}\ \mathrm{Pa}, \\ K_2 &= 2A\frac{\nu E}{(1+\nu)(1-2\nu)}\ \frac{\mathrm{N}}{\mathrm{m}^3}, \end{aligned}$$

where A [1/m] is a constant. The analytical solution to the above problem reads

$$\boldsymbol{u}_{\mathrm{S}} = \begin{bmatrix} -2Ax_1x_2 \\ Ax_1^2 \end{bmatrix}.$$

Further, plain strain ($\varepsilon_{33} = 0$) was assumed in the derivation. To see the influence of the second part of the stabilizing term, i.e., the λ-term, we calculate the error for different ν with and without the λ-term. The minimum of the error for different ν occurs for $C \approx 1.5$ when the λ-term is included, see Figure 4a. When the λ-term is dropped the minimums of the errors are not the same for different ν, see Figure 4b. The computed displacement to the model problem with all terms included for $C = 0.01$ and $C = 1.5$ can be seen in Figure 6. For $C = 0.01$ the elements rotate around their side nodes. To demonstrate that locking is avoided when the λ-term is dropped, we solve a problem on the unit square with the following (non-physical) displacement boundary conditions

$$\begin{aligned} \boldsymbol{u}_{\mathrm{S}}(0, x_2) &= \mathbf{0}, & \boldsymbol{u}_{\mathrm{S}}(1, x_2) &= \mathbf{0}, \\ \boldsymbol{u}_{\mathrm{S}}(x_1, 0) &= \mathbf{0}, & \boldsymbol{u}_{\mathrm{S}}(x_1, 1) &= [1, 0]^{\mathrm{T}}. \end{aligned}$$

Poisson's ratio is chosen as $\nu = 0.499$ and $C = 1.5$. As can be seen in Figure 5 locking occurs when the λ-term is included in the FE-formulation. The locking phenomena appears as oscillations in the displacement field

Remark: Note that even though we obtain less accurate solutions for certain ranges of C, the convergence rate, which is optimal in energy norm ($O(h)$) and L_2–norm ($O(h^2)$) (cf. [5]), will not be affected. The choice of C only affects the solution on a fixed mesh.

5.2. **Structural eigenvalue problem.** To further examine the properties of the proposed structural FE formulation, we solve the structural eigenvalue problem arising from the model problem given in Figure 7 with vacuum inside. Poisson's ratio is set to $\nu = 0.35$ and the stability parameter to $C = 1.5$. The computed eigenfrequencies are compared with the extrapolated eigenfrequencies, referred to as the 'exact', given in [2]. The result is seen in Table 1.

5.3. **Fluid–structure interaction example.** To investigate the proposed method's ability to solve fluid–structure interaction problems we solve the coupled eigenvalue problem arising from the configuration in Figure 7. Poisson's ratio is set to $\nu = 0.35$ and the stability parameter to $C = 1.5$. The computed eigenfrequencies are compared with the extrapolated eigenfrequencies, referred to as the 'exact', given in [2], and can be seen in Table 2. The displaced structure and the displacement field of the enclosed fluid for three eigenmodes are seen Figure 8.

6. Conclusions

A nonconforming finite element method for solving small vibration fluid–structure interaction was proposed. The fluid was discretized using the lowest order Raviart–Thomas element, and the structure was discretized using the first order Crouzeix–Raviart element with the unknowns defined as the normal and tangential projection of the displacement at the side nodes. These elements in combination with meshes that matched on the interface, led to that the normal displacement degrees of freedom were the same for the fluid and the structure. Thus conditions which related the normal displacement degrees of freedom on the interface did not have to be introduced. Further, a consistent stabilizing term was added to the weak form to make the Crouzeix–Raviart element stable for elasticity.

Numerical examples were given in order to demonstrate the method's ability to solve eigenvalue problems arising from structural dynamics and fluid–structure interaction. The results were compared with results given in [2]. Further, a numerical example showed that the stabilized Crouzeix–Raviart element works for near incompressible materials as proven in [5].

Acknowledgement

I would like to thank Professor Peter Hansbo for fruitful discussions on this research.

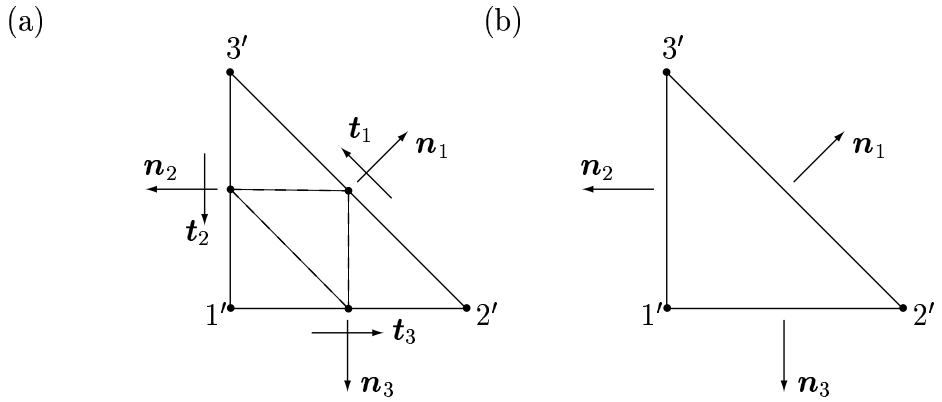

FIGURE 1. (a) The first order Crouzeix–Raviart element, the location of the unknowns (on the center of gravity of the element sides) and the directions of the unknowns. (b) The lowest order Raviart–Thomas element and the directions of the unknowns.

REFERENCES

[1] M. A. Hamdi, Y. Ousset, G. Verchery. A Displacement Method for the Analysis of Vibrations of Coupled Fluid–Structure Systems. *International Journal for Numerical Methods in Engineering* 1978; **13**:139–150.

[2] A. Bermúdez, R. Rodríguez. Finite Element Computation of the Vibration Modes of a Fluid–Soil System. *Computer Methods in Applied Mechanics and Engineering* 1994; **119**:355–370.

[3] A. Bermúdez, R. Durán, M. A. Muschietti, R. Rodríguez, J. Solomin. Fluid-Structure Finite Element Vibration Analysis of Fluid–Solid Systems without Spurious Modes. *SIAM Journal on Numerical Analysis* 1995; **32**:1280–1295.

[4] R. E. Ewing, O. Sævareid, J. Shen. Discretization schemes on triangular grids. *Computer Methods in Applied Mechanics and Engineering* 1998; **152**:219–238.

[5] P. Hansbo, M. G. Larson. Discontinuous Galerkin and the Crouzeix-Raviart Element: Application to Elasticity. *Research report Preprint 2000-09*; Chalmers Finite Element Center, Chalmers University of Technology, Göteborg Sweden 2001.

[6] P. Hansbo, M. G. Larson. Discontinuous Galerkin methods for incompressible and nearly incompressible elasticity by Nitsche's method. *Computer Methods in Applied Mechanics and Engineering* 2002; **191**:1895–1908.

[7] S. C. Brenner. Korn's Inequalities for Piecewise H^1 Vector Fields. *Industrial Mathematics Institute Research Report 2002:05*; Department of Mathematics, University of South Carolina.

[8] F. Thomasset. Implementation of Finite Element Methods for Navier-Stokes Equations. Springer Verlag, New York, 1981.

[9] X. Wang, K. Bathe. Displacement/Pressure Based Mixed Finite Element Formulation for Acoustic Fluid–Structure Interaction Problems. *International Journal for Numerical Methods in Engineering* 1997; **40**:2001–2017.

[10] T. J. R. Hughes. The Finite Element Method: Linear Static and Dynamic Finite Element Analysis. Prentice-Hall, New Jersey, 1987.

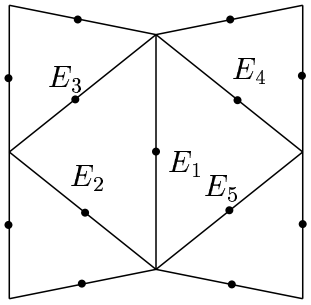

FIGURE 2. A structural element patch and its element sides $E_1 - E_5$.

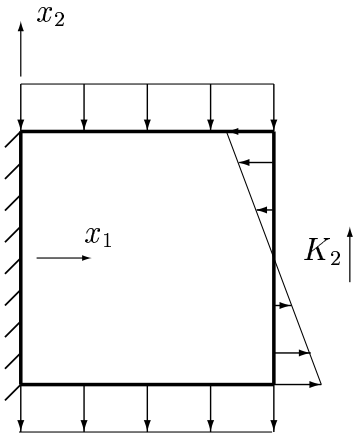

FIGURE 3. Test problem with the dimension $B \times H$ and the acting forces.

(a) (b)

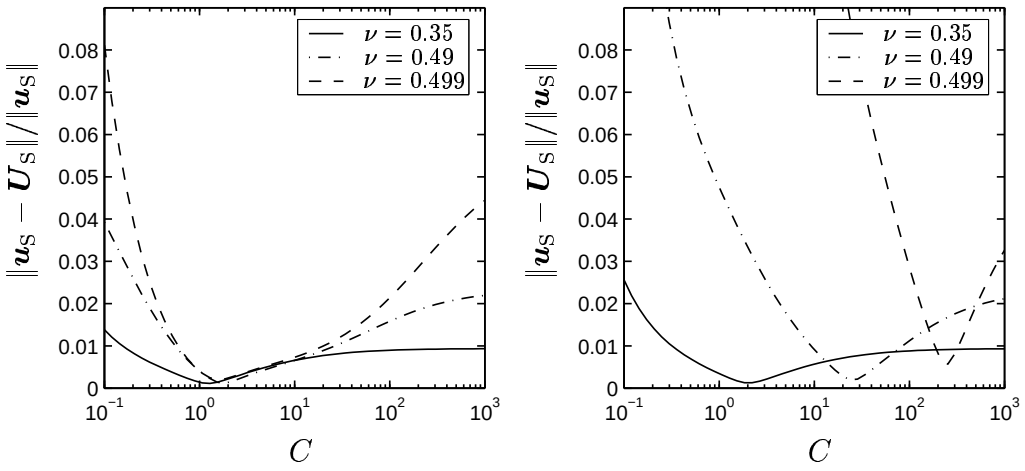

FIGURE 4. The normalized error to the test problem in Figure 3 using the proposed FE method, with the λ-term (a) included and (b) excluded

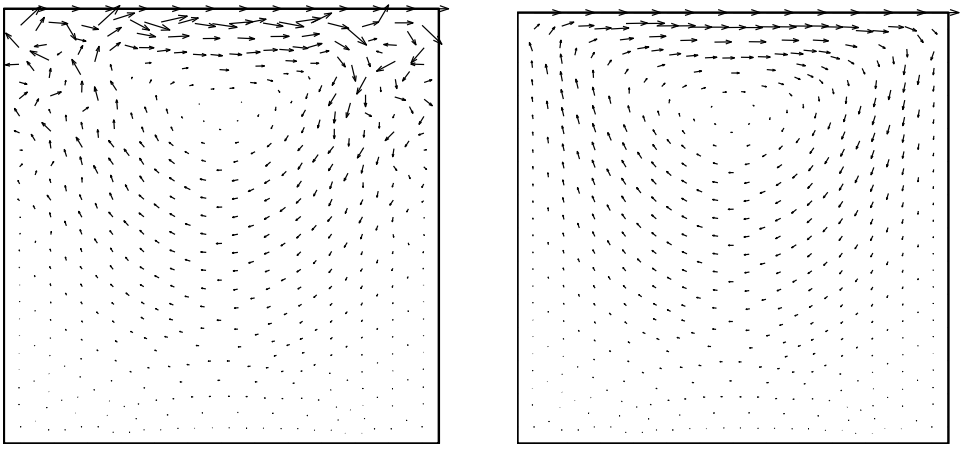

FIGURE 5. Structural example with $\nu = 0.499$. Formulation according to Equation (3.1) with the λ-term included (left) and excluded (right).

TABLE 1. The computed structural eigenfrequencies [Hz] compared with the 'exact' eigenfrequencies given in [2].

Mode	Computed	'Exact'	Error [%]
1	106.7	106.0	0.65
2	366.6	363.6	0.82
3	610.8	605.3	0.91
4	620.7	617.5	0.52
5	718.4	717.4	0.14
6	875.6	870.7	0.56
7	1220.3	1204.1	0.13
8	1224.1	1216.1	0.65
9	1649.5	1635.2	0.88

TABLE 2. The computed eigenfrequencies [Hz] to the coupled problem compared with the extrapolated eigenfrequencies given in [2].

Mode	Computed	'Exact'	Error [%]
1	105.0	102.2	2.78
2	343.7	336.8	2.04
3	547.0	509.5	7.35
4	620.4	605.4	2.46
5	671.7	670.3	0.20
6	748.7	746.1	0.34
7	821.7	820.5	0.14
8	866.5	857.2	1.09
9	998.6	993.0	0.56

(a)

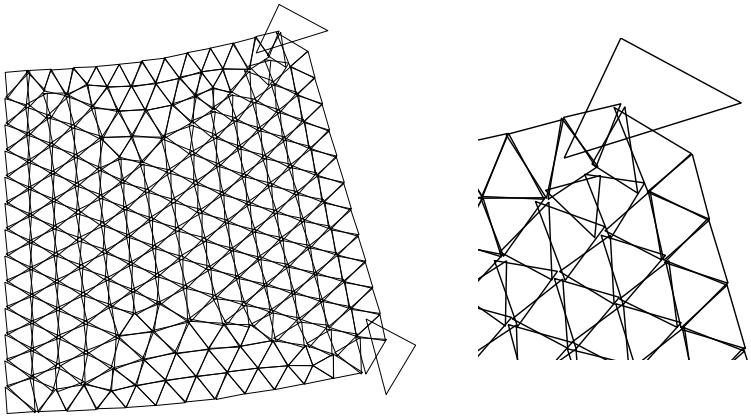

(b)

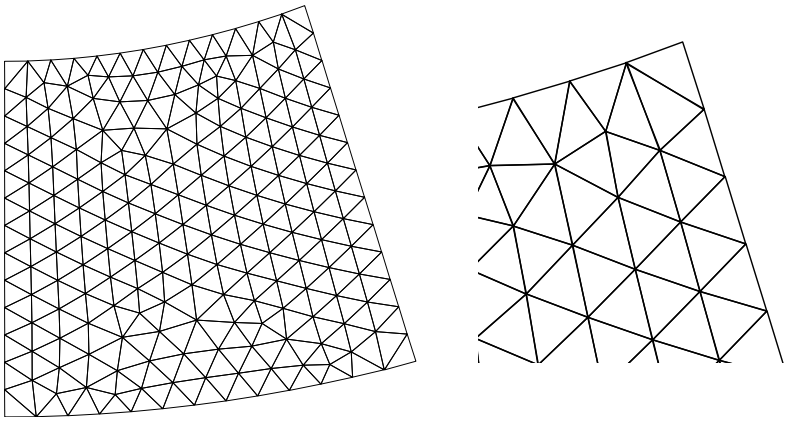

FIGURE 6. Numerical results of the computation with the structural configuration in Figure 3 with different values of the stabilizing parameter C, see Equation (3.1). (a) $C = 0.01$. (b) $C = 1.5$.

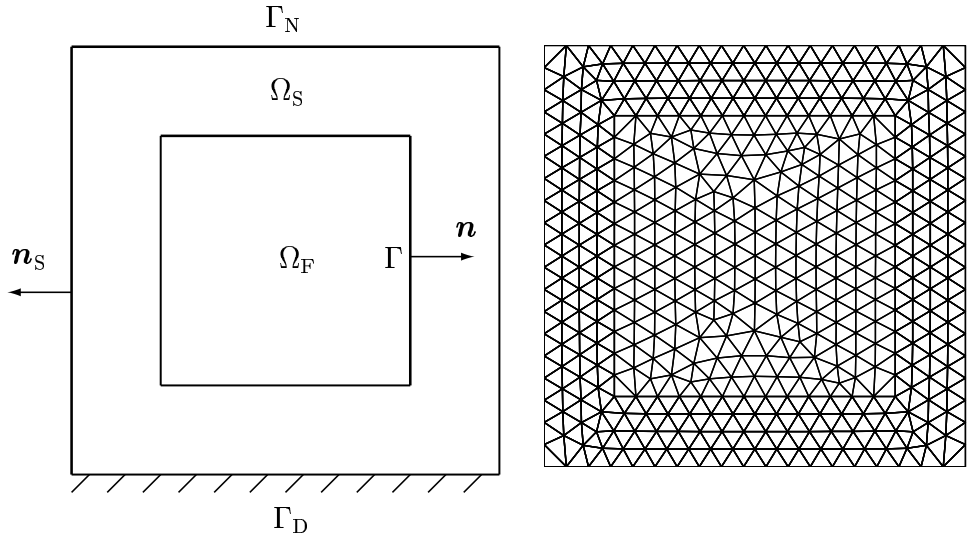

FIGURE 7. Fluid enclosed in a structure (left) and the meshed domains (right). The outer dimensions are $1.5 \times 1.5\,\mathrm{m}^2$ and the inner are $1 \times 1\,\mathrm{m}^2$.

(a)

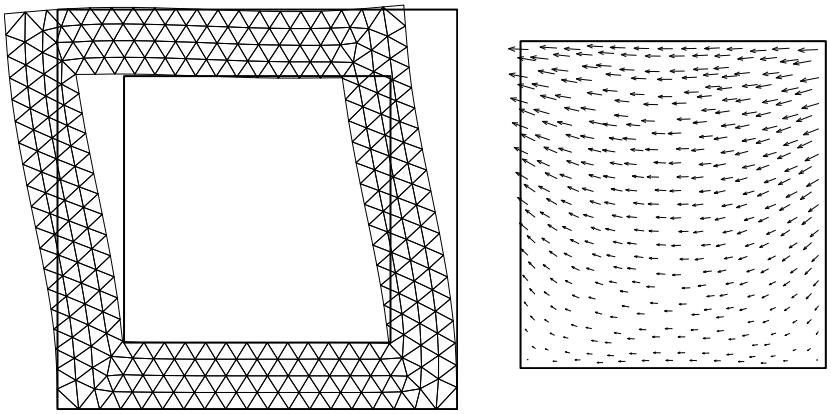

(b)

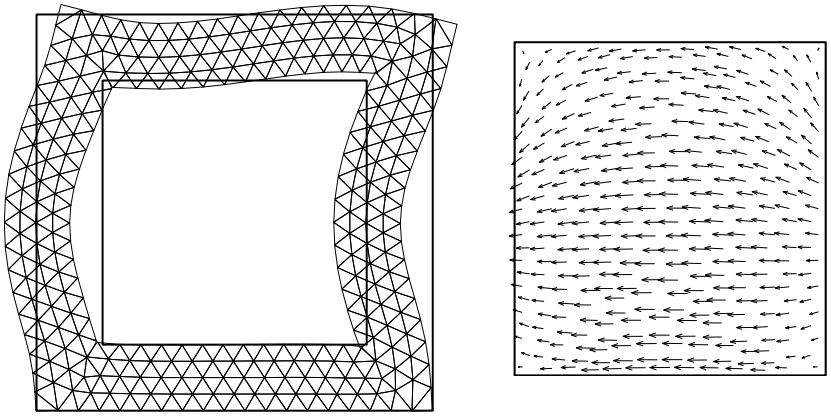

(c)

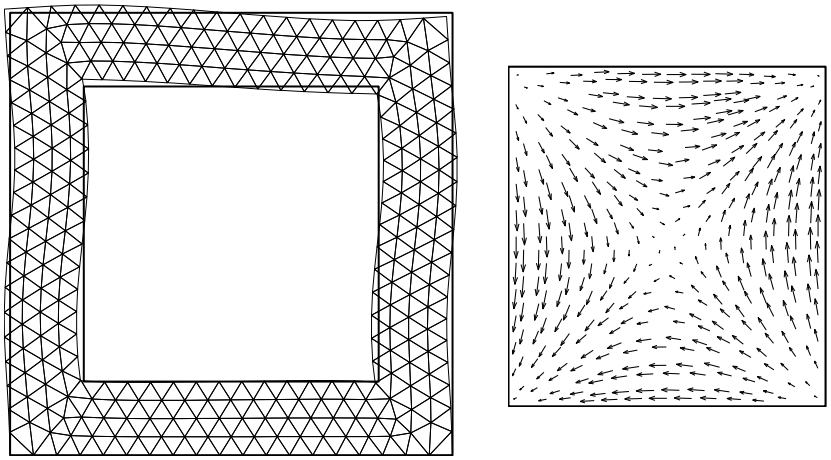

FIGURE 8. Eigenmodes of the coupled problem in Figure 7. The displaced structure (left) and the displacement field of the enclosed fluid (right). (a) The first eigenmode, (b) the third eigenmode, and (c) the ninth eigenmode.

Chalmers Finite Element Center Preprints

2001–01 *A simple nonconforming bilinear element for the elasticity problem*
Peter Hansbo and Mats G. Larson

2001–02 *The $\mathcal{LL}^*$ finite element method and multigrid for the magnetostatic problem*
Rickard Bergström, Mats G. Larson, and Klas Samuelsson

2001–03 *The Fokker-Planck operator as an asymptotic limit in anisotropic media*
Mohammad Asadzadeh

2001–04 *A posteriori error estimation of functionals in elliptic problems: experiments*
Mats G. Larson and A. Jonas Niklasson

2001–05 *A note on energy conservation for Hamiltonian systems using continuous time finite elements*
Peter Hansbo

2001–06 *Stationary level set method for modelling sharp interfaces in groundwater flow*
Nahidh Sharif and Nils-Erik Wiberg

2001–07 *Integration methods for the calculation of the magnetostatic field due to coils*
Marzia Fontana

2001–08 *Adaptive finite element computation of 3D magnetostatic problems in potential formulation*
Marzia Fontana

2001–09 *Multi-adaptive galerkin methods for ODEs I: theory & algorithms*
Anders Logg

2001–10 *Multi-adaptive galerkin methods for ODEs II: applications*
Anders Logg

2001–11 *Energy norm a posteriori error estimation for discontinuous Galerkin methods*
Roland Becker, Peter Hansbo, and Mats G. Larson

2001–12 *Analysis of a family of discontinuous Galerkin methods for elliptic problems: the one dimensional case*
Mats G. Larson and A. Jonas Niklasson

2001–13 *Analysis of a nonsymmetric discontinuous Galerkin method for elliptic problems: stability and energy error estimates*
Mats G. Larson and A. Jonas Niklasson

2001–14 *A hybrid method for the wave equation*
Larisa Beilina, Klas Samuelsson and Krister Åhlander

2001–15 *A finite element method for domain decomposition with non-matching grids*
Roland Becker, Peter Hansbo and Rolf Stenberg

2001–16 *Application of stable FEM-FDTD hybrid to scattering problems*
Thomas Rylander and Anders Bondeson

2001–17 *Eddy current computations using adaptive grids and edge elements*
Y. Q. Liu, A. Bondeson, R. Bergström, C. Johnson, M. G. Larson, and K. Samuelsson

2001–18 *Adaptive finite element methods for incompressible fluid flow*
Johan Hoffman and Claes Johnson

2001–19 *Dynamic subgrid modeling for time dependent convection–diffusion–reaction equations with fractal solutions*
Johan Hoffman

2001–20 *Topics in adaptive computational methods for differential equations*
Claes Johnson, Johan Hoffman and Anders Logg

2001–21 *An unfitted finite element method for elliptic interface problems*
Anita Hansbo and Peter Hansbo

2001–22 *A P^2–continuous, P^1–discontinuous finite element method for the Mindlin-Reissner plate model*
Peter Hansbo and Mats G. Larson

2002–01 *Approximation of time derivatives for parabolic equations in Banach space: constant time steps*
Yubin Yan

2002–02 *Approximation of time derivatives for parabolic equations in Banach space: variable time steps*
Yubin Yan

2002–03 *Stability of explicit-implicit hybrid time-stepping schemes for Maxwell's equations*
Thomas Rylander and Anders Bondeson

2002–04 *A computational study of transition to turbulence in shear flow*
Johan Hoffman and Claes Johnson

2002–05 *Adaptive hybrid FEM/FDM methods for inverse scattering problems*
Larisa Beilina

2002–06 *DOLFIN - Dynamic Object oriented Library for FINite element computation*
Johan Hoffman and Anders Logg

2002–07 *Explicit time-stepping for stiff ODEs*
Kenneth Eriksson, Claes Johnson and Anders Logg

2002–08 *Adaptive finite element methods for turbulent flow*
Johan Hoffman

2002–09 *Adaptive multiscale computational modeling of complex incompressible fluid flow*
Johan Hoffman and Claes Johnson

2002–10 *Least-squares finite element methods with applications in electromagnetics*
Rickard Bergström

2002–11 *Discontinuous/continuous least-squares finite element methods for elliptic problems*
Rickard Bergström and Mats G. Larson

2002–12 *Discontinuous least-squares finite element methods for the Div-Curl problem*
Rickard Bergström and Mats G. Larson

2002–13 *Object oriented implementation of a general finite element code*
Rickard Bergström

2002-14 *On adaptive strategies and error control in fracture mechanics*
Per Heintz and Klas Samuelsson

2002-15 *A unified stabilized method for Stokes' and Darcy's equations*
Erik Burman and Peter Hansbo

2002-16 *A finite element method on composite grids based on Nitsche's method*
Anita Hansbo, Peter Hansbo and Mats G. Larson

2002-17 *Edge stabilization for Galerkin approximations of convection–diffusion problems*
Erik Burman and Peter Hansbo

2002-18 *Adaptive strategies and error control for computing material forces in fracture mechanics*
Per Heintz, Fredrik Larsson, Peter Hansbo and Kenneth Runesson

2002-19 *A variable diffusion method for mesh smoothing*
J. Hermansson and P. Hansbo

2003-01 *A hybrid method for elastic waves*
L.Beilina

2003-02 *Application of the local nonobtuse tetrahedral refinement techniques near Fichera-like corners*
L.Beilina, S.Korotov and M. Křížek

2003-03 *Nitsche's method for coupling non-matching meshes in fluid-structure vibration problems*
Peter Hansbo and Joakim Hermansson

2003-04 *Crouzeix–Raviart and Raviart–Thomas elements for acoustic fluid–structure interaction*
Joakim Hermansson

These preprints can be obtained from

`www.phi.chalmers.se/preprints`